NASA
Technical
Memorandum

NASA TM - 86526

An Integrated Development Facility for the
Calibration of Low-Energy Charged Particle
Flight Instrumentation

Center Director's Discretionary Fund Final Report

By Alan P. Biddle and John M. Reynolds

Space Science Laboratory
Science and Engineering Directorate

October 1985

NOV 1985
RECEIVED

N86-22914

Unclas
04798

(NASA-TM-86526) AN INTEGRATED DEVELOPMENT
FACILITY FOR THE CALIBRATION OF LOW-ENERGY
CHARGED PARTICLE FLIGHT INSTRUMENTATION
Center Director's Discretionary Fund, Final
Report (NASA) 24 p HC A02/MF A01 CSCL 14B G3/35

NASA
National Aeronautics and
Space Administration

George C. Marshall Space Flight Center

MSFC · Form 3190 (Rev. May 1983)

1. REPORT NO. NASA TM- 86526	2. GOVERNMENT ACCESSION NO.	3. RECIPIENT'S CATALOG NO.
4. TITLE AND SUBTITLE An Integrated Development Facility for the Calibration of Low-Energy Charged Particle Flight Instrumentation - Center Director's Discretionary Fund Final Report		5. REPORT DATE October 1985
		6. PERFORMING ORGANIZATION CODE ES53
7. AUTHOR(S) Alan P. Biddle and John M. Reynolds		8. PERFORMING ORGANIZATION REPORT #
9. PERFORMING ORGANIZATION NAME AND ADDRESS George C. Marshall Space Flight Center Marshall Space Flight Center, Alabama 35812		10. WORK UNIT NO.
		11. CONTRACT OR GRANT NO.
		13. TYPE OF REPORT & PERIOD COVERED
12. SPONSORING AGENCY NAME AND ADDRESS National Aeronautics and Space Administration Washington, D.C. 20546		Technical Memorandum
		14. SPONSORING AGENCY CODE

15. SUPPLEMENTARY NOTES

Prepared by Space Science Laboratory, Science and Engineering Directorate.

16. ABSTRACT

A system has been developed specifically for the calibration and development of thermal ion instrumentation. The system is optimized to provide an extended beam (approximately 80 cm^2) with usable current rates, ~1 pA/cm^2, at beam energies as low as 1 eV, with much higher values available with increasing energy. The beam energy spread is typically less that 2 eV/charge, and the average angular divergence is approximately 2.5 deg. A tandem electrostatic and variable geometry magnetic mirror configuration within the ion source optimizes the use of the ionizing electrons, thus decreasing the gas and non-thermal electron throughput to the instrument chamber while improving the current density uniformity. The system is integrated under microcomputer control to allow automatic control and monitoring of the beam energy and composition and the mass- and angle-dependent response of the instrument under test. The data can be transmitted in nearly real-time to the interested investigators for comparison with expected results over existing computer networks. The system is pumped by a combination of carbon vane and cryogenic sorption roughing pumps and ion and liquid helium operating pumps. This allows testing and final calibration of flight instrumentation in an ultraclean environment.

17. KEY WORDS Ions, Source, Calibration, Automation, Magnetosphere	18. DISTRIBUTION STATEMENT Unlimited--Unclassified

19. SECURITY CLASSIF. (of this report) Unclassified	20. SECURITY CLASSIF. (of this page) Unclassified	21. NO. OF PAGES 23	22. PRICE NTIS

MSFC - Form 3292 (May 1969)

ACKNOWLEDGMENTS

TABLE OF CONTENTS

LIST OF ILLUSTRATIONS

TECHNICAL MEMORANDUM

AN INTEGRATED DEVELOPMENT FACILITY FOR THE CALIBRATION
OF LOW-ENERGY CHARGED PARTICLE FLIGHT INSTRUMENTATION -
CENTER DIRECTOR'S DISCRETIONARY FUND FINAL REPORT

I. INTRODUCTION

Recent advances in space plasma physics with the current generation of thermal ion instruments have brought about an enhanced appreciation of the importance of thermal plasmas in many important areas such as energy transport and wave-particle interactions [1-2]. These core plasmas, typically with energies below 100 eV, are subject to complexities of analysis not found at higher energies. External to the instrument, the spacecraft potential in low density areas, such as in the polar wind, is often comparable to the particle kinetic energy, with profound effects on both the effective instrument solid angle and the rejection of particles below this energy [3]. Several techniques such as aperture plane biasing [4] and ion emitters for potential control [5] have been used or proposed, and numerous analytical [6] and semi-empirical methods [7] have been developed to successfully analyze this data. Most such procedures require, or are simplified by, an accurate laboratory characterization of the instrument.

However, even in regions of space with sufficiently high plasma density where spacecraft charging can be ignored, there is a great challenge in determining the response of the instrument itself. Below about 10 eV, certain physical effects become significant in both the instrument under test and in the calibration facility. In the instrument, the effective area and solid angle can be decreased by image charge effects. The potentials induced near conducting surfaces are typically a few volts, equal to or even greater than the particle energy in the spacecraft reference frame. Also some sophisticated instruments include multifunction elements in the beam path that are partially transparent with unscreened holes [4]. This configuration can form a strongly converging lens when the particle energy is comparable to the adjacent electrode potentials [8]. While the actual optics of this configuration are valuable techniques for increasing the instrument sensitivity, they are difficult if not impossible to calculate in practice. Equivalent effects in laboratory facilities are found in energy and mass selectors, beam deflection mechanisms, collimating apertures, etc. Likewise, the effective transparency of gridded energy analyzers is a strong function of the type of grid material used, and of the geometry of the adjacent grids [9].

In addition to solid angle effects, the effective area can be subject to variation with the counting rate because of non-linearities in the detector systems. If the ratio of counts vs. input particles is known over more than the full range of expected operating parameters, the usable dynamic range can be extended far beyond the range where saturation begins. In fact, with sufficiently detailed knowledge, it is possible to recover data where the

indicated rate falls with increasing input. For example, this situation can be encountered during perigee passes in the plasmasphere. These and other competing instrument effects can be modeled (both piecewise and as a system) to guide design and construction of the instrument. Ultimately, the completed system must be calibrated with as little as possible of the instrument response left to extrapolation. This is especially true at both the highest and lowest counting regimes and at the minimum particle energy.

These considerations dictate the basic approach to the system design. In order to insure usable currents at minimum angular divergence, we have designed a system optimized for use in the critical range below 10 eV. The philosophy is to build a system with a minimum of preprocessing of the beam, and then make detailed analysis of the beam at the point it enters the instrument. This reduces the beam attenuation and decreases somewhat the uncertainties of trying to infer the final beam parameters from remote measurements. Direct measurements are made of the beam energy and composition with a retarding energy analyzer and an ion mass spectrometer (IMS) located near the plane of the instrument entrance aperture. This system, and its predecessors, has been used to calibrate and develop such instruments as the Light Ion Mass Spectrometer (LIMS) [10] and the Retarding Ion Mass Spectrometer (RIMS) [4], and is currently being used to develop the Thermal Ion Dynamics Experiment for the International Solar Terrestrial Program. Table 1 shows the typical range of parameters covered by this facility.

TABLE 1. PERFORMANCE RANGE OF CALIBRATION FACILITY

PARAMETER	OPERATIVE VALUES
Energy Range	1-150 eV/charge
Energy Spread	
Min	0.6 eV/charge
Max	3.5 eV/charge
Typical	1.1 eV/charge
Beam Cross Section	15 cm (FWHM)
Beam Uniformity	8% typical over central 10 cm
Intensity	>108 #/cm^2 (E > 10 eV)
	>106 #/cm^2 (10 eV > 1 eV)
Vacuum Base Pressure	10^{-8} torr
Maximum Instrument Parameters	
Height	38 cm
Width	38 cm
Mass	9 kg

II. INSTRUMENTATION

A. Overview

Figure 1 shows a block diagram of the Low-Energy Ion Facility (LEIF). Ions are produced in an electron bombardment ion source with an effective circular aperture of 8-cm-diameter, and then passed through a series of electrostatic lenses in the active and passive drift spaces. The beam is then imaged to the plane of the admittance aperture of the object under test. Beam current, energy, energy spread, and composition are periodically sampled and fed back for active control of the ion source, as well as made available for comparison with the instrument under test. The instrument is located in a turntable which allows the instrument to be tilted ±90 deg, and rotated ±180 deg. Additionally, the instrument can be simultaneously translated in the X-Y entrance plane of the tilt table, thus allowing the full response of large aperture instruments to be mapped without requiring multiple access to the chamber. These four degrees of motion are under computer control and can be used to allow data to be taken in the natural coordinates of the instrument under test by the appropriate coordinate transformations. The normal base pressure of the instrument chamber is typically in the 10^{-8} torr region. Outgassing from the test article, and feedthrough from the source working gas, usually raises the pressure to the upper 10^{-7} range.
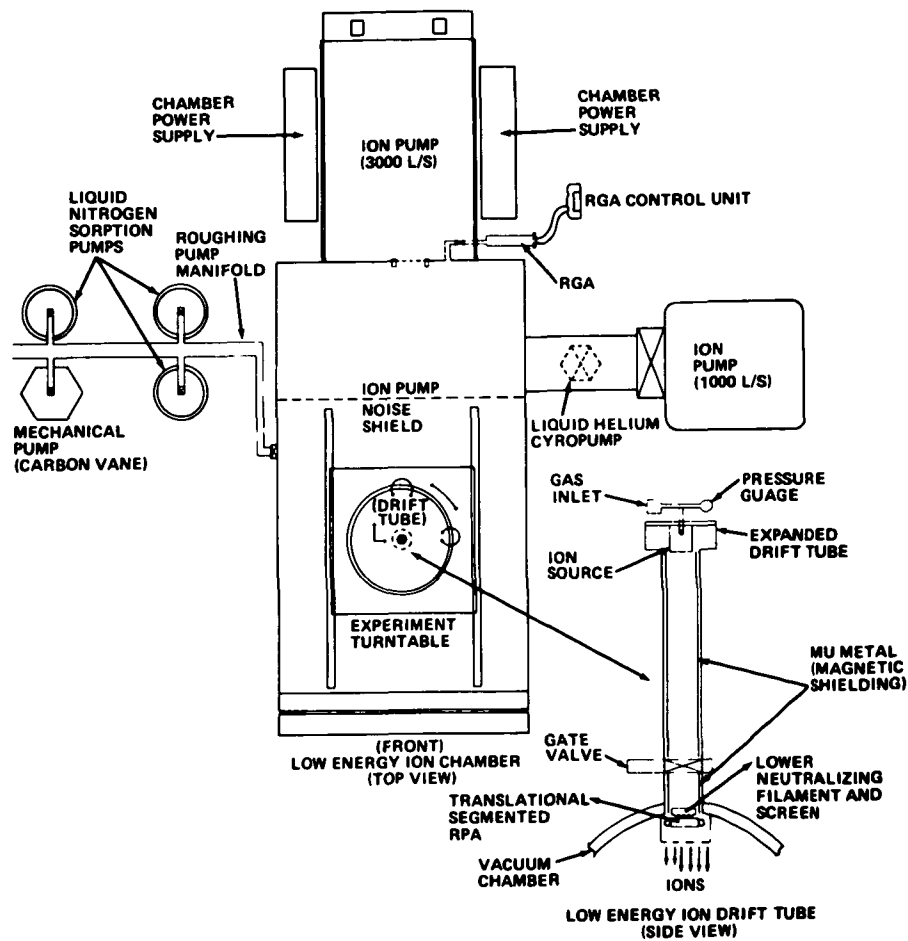

Figure 1. Block diagram of the Low-Energy Ion Facility (LEIF).

3

B. Ion Source

The ion source shown in Figure 2 is derivative of a Kaufman thruster [11] in that a directly-heated cathode provides electrons used to produce ions by impact ionization, and an externally applied magnetic field increases the path length the electrons follow before they can exit the ionization region. Several enhancements have been made to this basic design to make it more suitable to producing an extended, nearly monoenergetic beam suitable for instrument calibration.
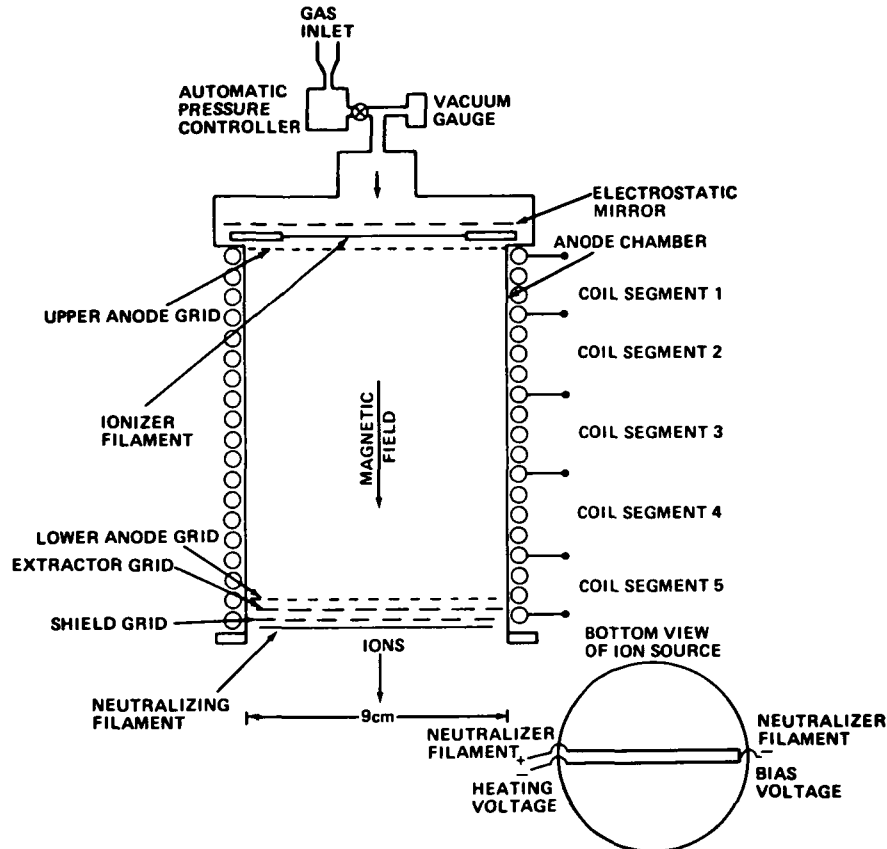

Figure 2. Expanded view ion source.

A primary concern for instrument calibration is that the ion beam be nearly monoenergetic. This allows the instrument response to be directly determined without the need to deconvolve finite temperature spreads. Since indirectly heated cathodes are unsuitable due to the reactive nature and relatively high pressures of the working gases, it is necessary to electrically isolate the electron source from the ionization region. Otherwise, a significant fraction of the ions will be created in a potential spread characteristic of the potential drop along the filament and the bias voltage applied to the filament. This isolation is achieved by making the ionization region an equipotential space consisting of a conducting cylinder with a 90% optically transparent conducting grid at the ionizer end. The mesh provides relatively unobstructed electron access but blocks the electric field. This cylinder is biased at the beam energy; though, for reasons discussed later,

the actual energy is typically about a volt below this value. Because the electrons are emitted essentially isotropically from the filament, a simple repeller grid, which constitutes an electrostatic mirror, is located behind the filament and biased at the most negative side of the filament. This provides a sufficiently strong electron potential barrier so that all but a few electrons are reflected back into the anode chamber region. The ions formed outside the anode chamber in the strong electric fields surrounding the filament potentials are repelled by the higher positive potential of the anode, thus preventing them from entering the extracted ion stream. Figure 3 shows the enhancement of the beam current with and without the reflector grid. At low critical beam energies, the gain is close the the expected factor of two, while it is somewhat less at higher energies. This is evidently the result of changing other parameters, such as the magnetic field topology and magnitude.
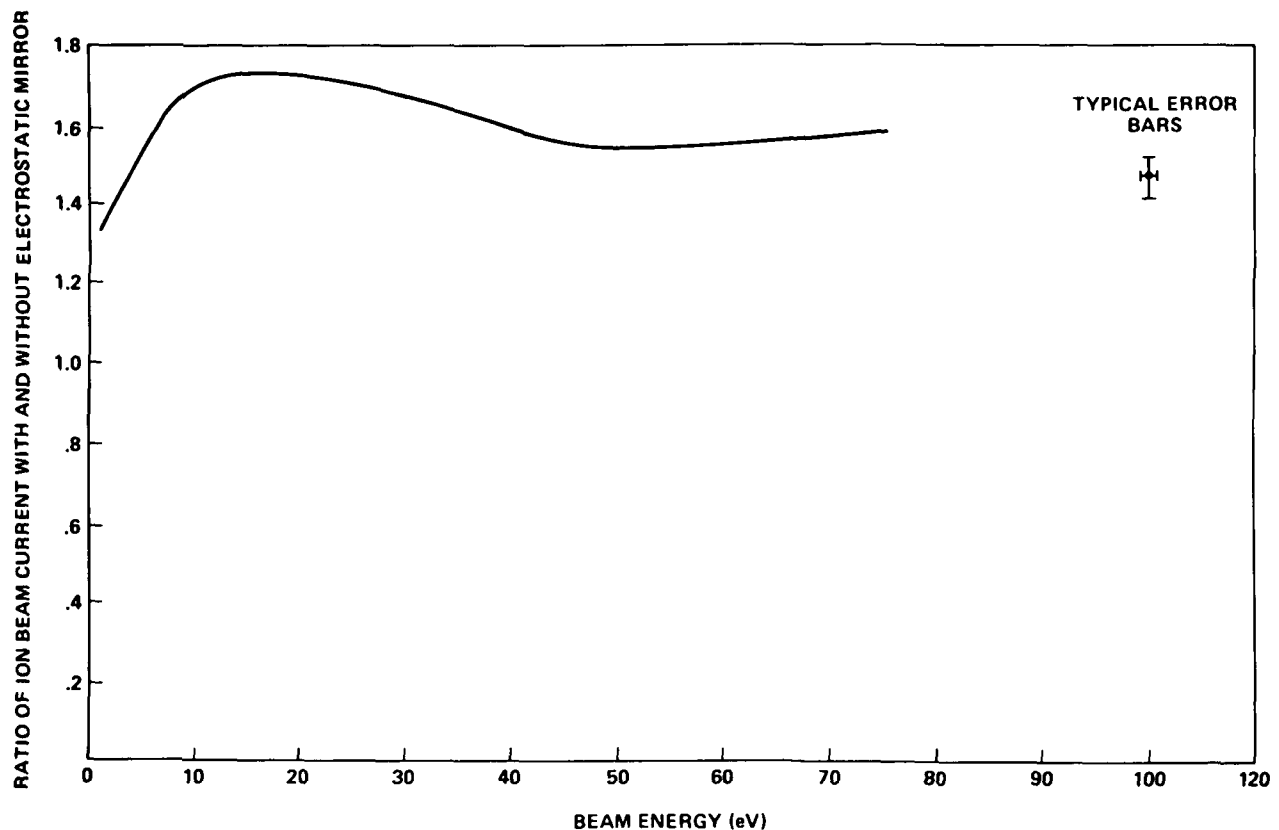
Figure 3. Ratio of beam current with and without electrostatic mirror vs. ion energy. The other source parameters are adjusted in each case for maximum output.

The configuration and location of the ionizer filament must be chosen with some care. Electrons ideally should be deposited uniformly on each cylindrical flux surface so as to provide a uniform volume ionization rate. Ignoring gyroradius and radial diffusion effects in a uniform solenoidal field, it can be easily shown that an appropriately chosen radial spiral shape

5

provides the required deposition. A more practical solution is to place a multiturn transverse spiral of filament wire across the diameter of the source. This arrangement, combined with the azimuthal drift of the electrons due to the magnetic field gradient and the various radially diffusive processes, gives a practical level of uniformity. The few electrons with sufficient radial energy to reach the walls are lost immediately adjacent to the filament. Since this surface is insulating, it quickly provides effective electrostatic self-shielding.

Since the ionization mean-free-path of the electrons is at least comparable to the scale length [12] of a typical impact ionization ion source, it has long been common to used a magnetic field to increase greatly the electron drift path. The parameters of the field are constrained by several factors. First, the resulting gyroradius of the electrons must be small compared with the source size. Additionally, the ideal field topology should be such as to provide a uniform distribution of electrons throughout the anode chamber to insure a uniform beam current density. Any non-ionizing electrons should be returned to a surface which will minimize impurity generation. These requirements are usually met using a magnetic field generated by permanent magnets [11]. Electrons are emitted on field lines in a high field region and then spread along the field lines toward the extraction end of the system. For this application, this approach poses a drawback in that any electrons that escape the source are injected into the test chamber as a highly non-thermal beam which can interfere with the test instrument. This is usually resolved by requiring the extractor grid to be more negative than the ionizer filament, often requiring extractor potentials that otherwise degrade the beam quality in terms of divergence and magnitude. Finally, it would be useful to allow a dynamic adjustment of the magnetic field magnitude and at least, in part, allow its topology to be changed to adjust for the requirements of changing beam currents, energy, and ionizer bias voltage.

These considerations have been substantively answered by the use of a five-segment solenoidal field coil. The typical strength of the field along the center axis is plotted in Figure 4. A converging magnetic mirror configuration rather than diverging field is used; the electrons are emitted in a relatively low magnetic field region. The electrons are launched directly, or after being reflected by the electrostatic mirror, with essentially a continuum of directions toward the ionization region. The energy spread consists of essentially the 10-V drop across the filament wire. The magnetic field rises slowly until the last solenoid section is encountered at the extractor end. Here, the electrons see a strong magnetic mirror which reflects the electrons back into the chamber. This tends to keep the fast electrons from the sheath region and minimizes the physical volume lacking ionizing electrons. The ions are essentially unaffected by the magnetic force and are weakly collisional with the ions and neutral particles, producing a nearly uniform current column. The inner side of the lower anode grid shows an approximately 2-cm-diameter mark, consistent with the normal magnetic field ratios. Under normal operating conditions, no fast electrons are found in the test chamber unless the mirror ratio is reduced to near unity.

The beam energy is operationally defined as the half current point in the retarding curve of the reference retarding potential analyzer, and is found to be typically several tenths of volts below the positive anode bias energy. This occurs because the plasma in the anode chamber is very weakly ionized;

6

IONIZER COIL

SEGMENT SEGMENT SEGMENT SEGMENT   SEGMENT
1   2   3   4   5

IONIZER
SOURCE
FILAMENT

EXTRACTOR
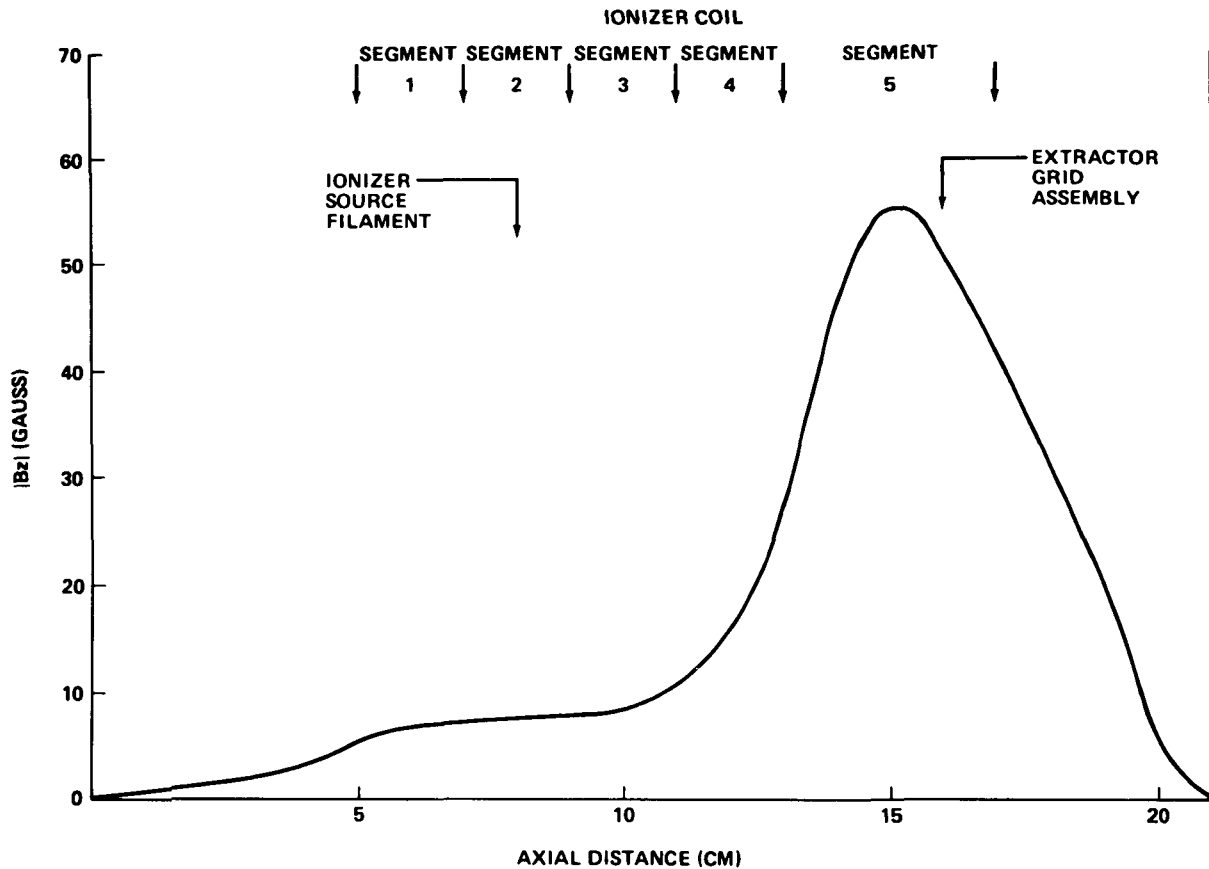GRID
ASSEMBLY

|Bz| (GAUSS)

AXIAL DISTANCE (CM)

Figure 4.   Typical axial magnetic field strength within ion source.

the ionization percentage is approximately 0.001%.   The fast electrons from the ionizer, confined by the combination of a relatively strong magnetic field and the ionizer and extractor grids which are negative with respect to the anode, can trap enough primary and secondary electrons to significantly depress the plasma potential in the anode chamber.   The deviation in the beam energy is found to be roughly proportional to the emission of the ionizer, and is easily compensated for by a slight increase in the anode potential.

Since the particle confinement times of the ions are very short compared to the electron-ion thermalization time, the beam energy spread should nominally be characterized by the neutral thermal energy, 0.025 eV.   In practice, it is usually at least a few thousand degrees in confined plasmas, due to the sheath potential drop effect found in many devices such as cusp confinement devices [13].   However, increasing the filament emission, which decreases the plasma potential, increases the energy spread.   This implies this mechanism is indeed the primary source of the spread.   It is worth noting that several effects have been documented which can interfere with the accurate measurement of the absolute beam energy, current, and spread.   These are discussed in, for example, references [8], [9], [13], [14], and especially [15].

This tandem mirror (a combination of an electrostatic mirror behind the electron source and a magnetic mirror near the extractor end) allows nearly 100% utilization of the primary electrons, while preventing the emission of a

7

beam of non-thermal electrons into the chamber unless specifically desired. This results in a minimum of working gas throughput which is especially helpful when using the ion and cryogenic pumps. Additionally, greater thermal stability and lifetime of the source results from the lowered power input to the source.

The extractor system consists of three grids (Figure 2). The inner anode grid is operated at the anode potential and constitutes one end of the ionization region. The middle grid is the extractor and is biased negatively to establish space charge-limited ion flow. For applications insensitive to the divergence angle, it is not necessary to include an outer grid. The original version of this source [16] performed well, even though the divergence angle was typically 30-45 deg. With a sufficiently long passive drift space, the ions actually arriving at the test instrument can have arbitrarily small divergence angles, but at the cost of the total flux.

The addition of a third, outside grid substantially reduces the beam divergence [17]. First, this provides a purely geometric collimation in the extractor assembly. Particles with trajectories significantly misaligned with the drift tube axis are lost between the grids. Additionally, this grid explicitly defines a critical equipotential surface. This yields far less diverging fringing fields, and in better collimation of the beam. At very high beam currents, Aston and Kaufman [17] have shown that the surface where quasineutralitiy is achieved is concave as seen from the ion source, which is also a diverging configuration.

C. Beam Neutralization

Charge neutralization of the beam is neither required nor possible at normal operating conditions. Typical densities are in the range of 0.1 to 1000 cm^{-3} to simulate ion fluxes encountered in the space environment. Under worse case conditions, 1 eV N_2^+, the beam potential is typically a few millivolts with respect to the chamber. This is small compared with even the thermionically emitted electrons, exclusive of any additional bias, and is incapable of trapping the electrons. Current neutralization is of course supported by the chamber walls.

Distributed sources of electrons can be useful. First, it is often necessary to operate at unrealistically high currents to determine the dynamic range of the instrument. There is often a modest but useful improvement in these operations with neutralization. A subsidiary reason for having filaments present is that the resulting cloud of electrons can generate a weak local potential well which can make a contribution in collimating the ion beam. With bias potentials comparable to the ionization potential on the filament, it becomes a source of ionizing electrons for the neutral gas flowing from the ion source. While the quality of the "beam" created is questionable, it is useful for generating a pseudo-Maxwellian plasma, either by itself or superimposed over the normal source output. Finally, with no gas flowing, the electrons can be extracted down the drift tube to produce a nearly monoenergetic electron beam with energies in the range of 10 to 150 eV. However, the small electron gyroradius tends to produce wide spreads in the effective arrival angles.

8

One neutralizer filament is installed in the standard location at the extractor end of the ion source. The wide range of working gases, including traces of oxygen and the need to cycle the ion source to ambient condition, precludes the use of an indirectly heated cathode so some large electric fields can be generated. The "hairpin configuration" allows nearly complete cancellation of the potential gradient along the wire, thus minimizing the deflection of the beam by the filament heating voltage. The transverse field that exists between the two wires is small. The "slice" deflected out of the beam is small, and the ion motion tends to fill in the space. The beam is uniform by the time it exits the drift tube. The strong magnetic field at the extractor end of the source simultaneously expells electrons, thus preventing them from entering the source, and by the action of the field gradient causes electrons be rotated azimuthally to provide a uniform cloud.

D. Drift Tube

The 1.4 m drift tube provides a space in which any "near field" irregularities in the beam are washed out and high divergence particles are lost. This drift region must be shielded against ambient magnetic fields to insure that the beam is not significantly deflected from normal incidence. For instance, a 1 eV proton beam has a measured deflection of approximately 5 deg from normal at the test instrument in the existing ambient building and terrestrial magnetic field. To reduce this field to about 1% of the ambient value, an electrically insulated sleeve of mu-metal, divided into two sections at the gate valve, is installed in the drift space. The combined stack also forms a series of electrostatic lenses to shape the beam and improve its collimation. In practice, the actual limiting factor at such low energies is the non-uniform potential and geometry of most instruments.

Figure 5 shows the drift tube configuration simplified and redrawn to emphasize the nature of the lenses formed [8]. The extractor end of the source is approximately flush with the upper mu-metal sleeve and constitutes the beginning of the lens system. The gun is operated several volts above the system ground at the beam energy, while the extractor is operated sufficiently negative with respect to the beam energy that it is near, or slightly below chamber ground but more positively than the shield grid. . The upper drift space sleeve is operated less positively than the beam energy with respect to the system ground. This forms the first converging lens. The sleeve then forms a drift space between the source and the gate valve. A second sleeve on the other side of the gate valve, also biased, forms a lens which can be thought of as a variation of the classical "einzel" lens. The optimum potential is usually intermediate between the upper sleeve and chamber ground. The cylinders on either side are of equal diameter, and the central "electrode" has a predominantly similar radius with a small 3 cm axial length of effectively an infinite radius. Alternatively, the system can be treated as a two-cylinder lens in which the gap between the cylinder is not small compared with the cylinder radius. In either case, the qualitatively converging properties of the lens are unchanged, though the analysis of non-paraxial particles is considerably more difficult. The lens at the end of the drift tube is somewhat more difficult to categorize. Qualitatively, it is close to being a two-cylinder lens of nearly equal diameter, formed by the lower mu-metal section and the lower section of the drift tube. An independently biasable screen is located at the junction of the two cylinders. This screen is normally operated at ground potential and provides a relatively well-defined equipotential

9

surface prior to the particles entering the chamber. A second filament, located at the end of the drift tube (Figure 1) is of similar construction. It does, however, lack the strong local magnetic field, making it suitable only for high density, non-critical operation.

$$E_{beam} \approx V_b > V\mu u \geqslant V\mu l \approx Vge \approx Vgs \approx 0$$
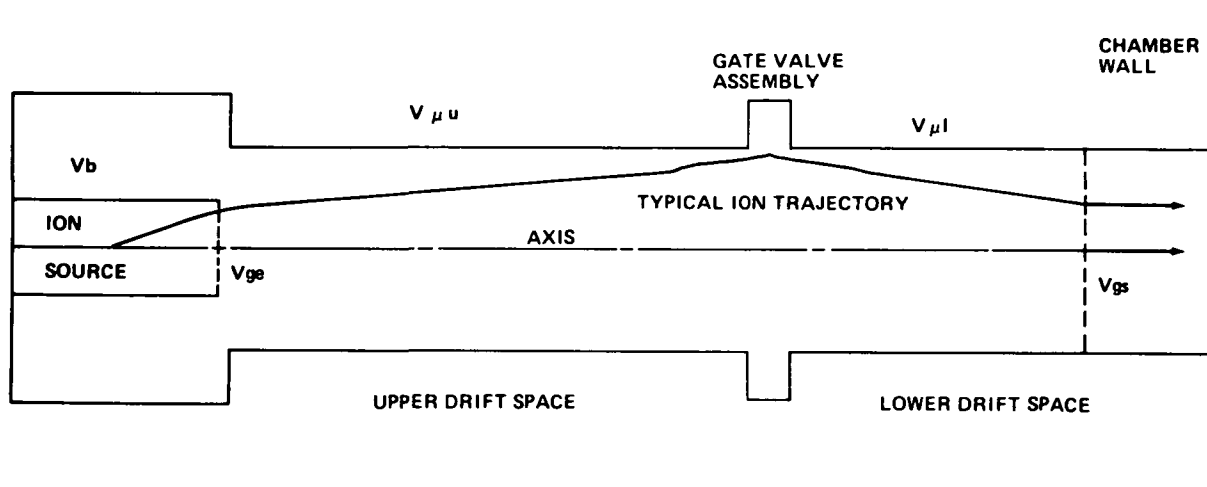
Figure 5. Schematic representation of the active drift space lenses.
An approximate trajectory is shown by the solid line.
The scale is 1:4 except for the upper drift space,
which is shown at 1:8.

This compound lens allows the full output of the source to be focused to a small circle of confusion at high energies. This is useful for situations uncritical as to arrival angle but requiring large currents. However, the output plane of the source is normally imaged to the input plane of the instrument for the greatest uniformity and minimum divergence. For tests requiring minimum divergence, such as electrostatic analyzers, the drift space is operated passively, though the flux delivered is about one to two orders of magnitude lower.

E. Beam Characterization

The total beam current delivered to the test instrument is measured by a conventional four-grid retarding potential analyzer (RPA). The current is measured at zero retarding potential directly by an electrometer in order to decrease the errors inherent in cross calibration, which would be required with an active counting system. A 2 cm^2 effective area is a good engineering compromise in covering the test article admittance aperture without extending outside the area of uniform current density. A second segmented RPA is available for insertion at the lower end of the drift tube. Its construction is similar to the calibration unit, however, it is larger in diameter and has a collector plate segmented into five sections. Each segment is masked by an aperture which gives an effective area of 0.83 cm^2. The centers of these apertures are at the center of the drift tube, and at four points on a surrounding circle. This assembly can be moved across the beam to check for

10

variations in the source output. In conjunction with the calibration de-
tector, it allows a direct measurement of the average beam divergence.

A reference IMS will be available for calibration of instruments with
mass resolution capability. The reference unit is mechanically nearly identi-
cal with that used in the RIMS on the Dynamics Explorer 1 spacecraft [4].
Briefly, it is a magnetic selector type with low and high mass detectors
covering the ranges of 1 to 4 eV/charge, and 4 to 64 AMU/charge, respectively.
The aperture of the IMS can be placed nearly coplanar with the device under
test, and the arriving ions are highly collimated. This configuration allows
absolute calibration by measuring the total ion current with the Faraday cup
and the apportioning of the flux of each ion in the ratio of the count rates.
The electronics have been simplified to allow for external control. A dif-
ferential multigrid energy analyzer is being developed for the IMS to deter-
mine the energy spread of the individual species.

F. Digital Control System

The computer system (Figure 6) used to both monitor and control the
system uses the IEEE-488 bus standard [18] for nearly all external inter-
facing. This bus, while of only moderate speed (approximately 250 kilobytes/
sec), possesses several advantages, especially when any equipment must be
integrated into the system operation quickly and cheaply. First, the hardware
and software interfaces are extremely well standardized. Most common general
laboratory instruments, such as digital counters, power supplies, digital
storage scopes, voltmeters, etc., are available with this interface. Software
drivers are available for most high level languages and any appropriate com-
puter. This allows an instrument to be installed and operating quickly, since
no hardware collimation is required. Second, typical interface specifications
provide for at least a 500-V isolation between the instrumentation and the
computer. This is ideal in situations where some power supplies are operated
at potentials different from the system ground. In addition to the ease of
integration, the typical resolution programmable for power supplies is 1 part
in 4096. For instance, this translates to a resolution of 0.24 mV in setting
and determining the beam energy.

In order to realize the maximum utility from a calibration system, it is
necessary to be able to automatically merge the data from the instrument with
that of the facility. Several undedicated RS-232 ports, discrete digital I/O
lines, and IEEE-488 addresses exist for this purpose. In normal use, the data
from the instrument are fed to the multitasking system controller. This data
can be temporarily archived with the simultaneous calibration system data, and
then networked over the Space Plasma Analysis Network (SPAN) [19] to the
appropriate institutions. A graphic "quick look" capability exists to monitor
the results for anomalies. The system controllers and computer, as well as
the user-supplied controllers, are supported by uninterruptable power sup-
plies. These provide additional isolation from noise transients and inoppor-
tune power failures.

G. Chamber and Vacuum Facilities

The experimental facility [15] is a cylindrical chamber 122 cm in diame-
ter and 183 cm long. Access to the chamber is by a 122 cm removable door on a
dolly for test article installation to allow full access. Baffles and ground
screen block the entrance of electrons from the ion pumps.

SPAN LINK

RS-232-C

| ION SOURCE POWER SUPPLIES | ION SOURCE BEAM MONITORS | TABLE α, β, X, Y CONTROL |

MICROCOMPUTER — **IEEE-488**

| VDT | PRINTER/ PLOTTER | UNDEDICATED INSTRUMENTS | DISCRETE CONTROL LINES | USER IEEE-488 INTERFACE |

ON LINE MASS STORAGE

EXPERIMENT

———— DEDICATED SYSTEM LINKS
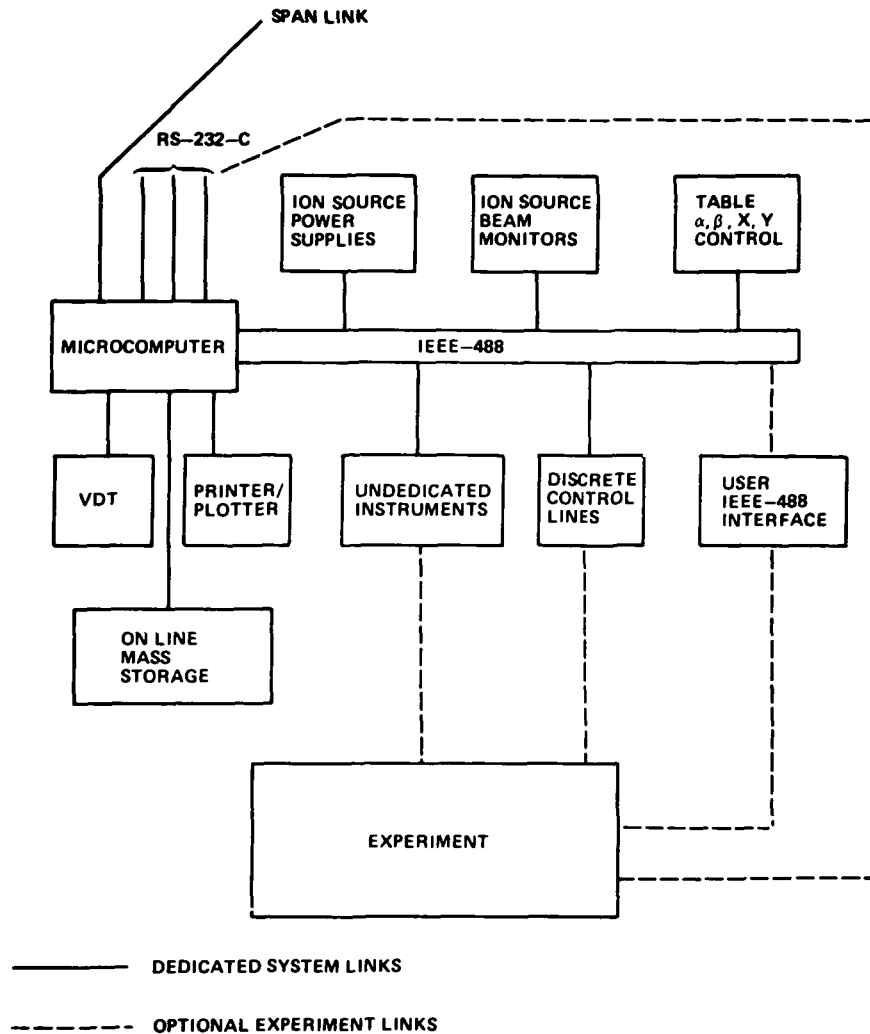
— — — — OPTIONAL EXPERIMENT LINKS

Figure 6. Block diagram of calibration and data control system. The RS-232-C and the IEEE-488 ports allow rapid addition of modular equipment as required.

III. PERFORMANCE

A. Beam Energy

This facility is optimized to produce high quality ion beams with a continuously adjustable range of energies up to 150 eV. This limit is imposed by the existing power supplies and the isolation requirements of the computer interface system. The minimum energy at which usable count rates are obtained is approximately 1 eV, though this limit is dependent on the effective area of the test instrument. Below 5 eV, the flux drops very rapidly (Figure 7) due to a combination of space charge limitations in the source, and the fact that the electrostatic mirrors are ineffective so close to the system ground potential. The beam energy spread is nearly constant at 1 to 2 eV. There is a weak peak near 50 eV in the energy spread, and a slow fall above and below this value.
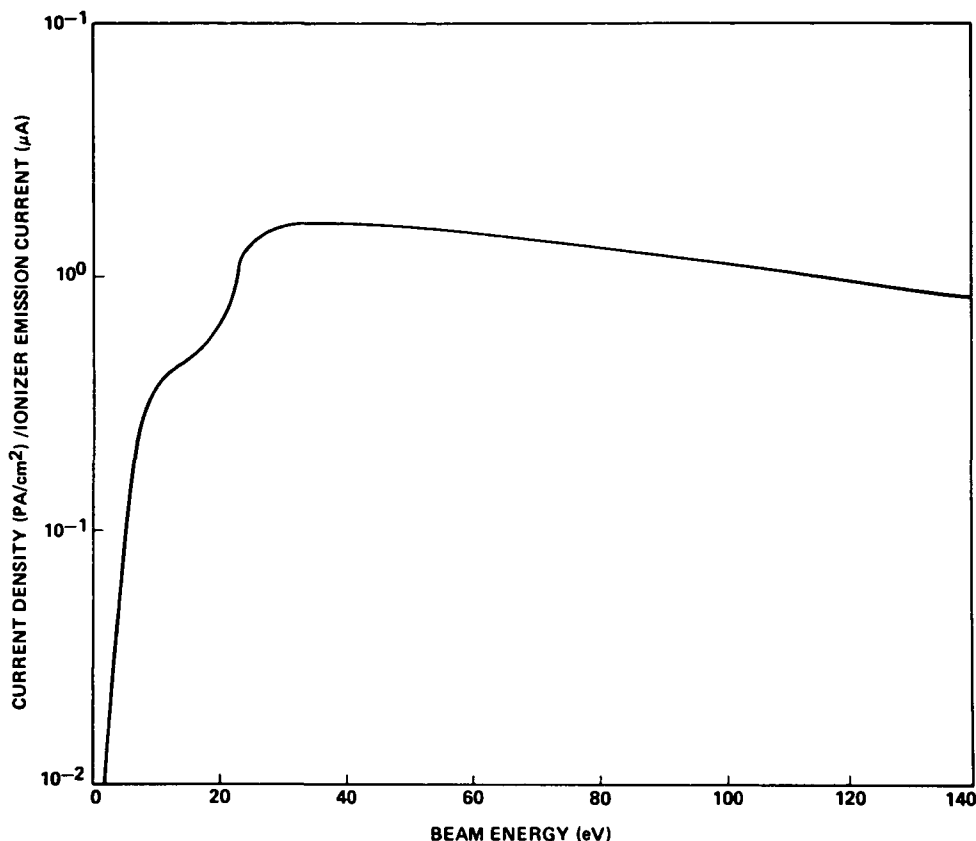
Figure 7. Current density per microamp of ionizer current
delivered to the test instrument vs. beam energy.

The energy of the beam can be swept over a range of approximately 20%
above 20 eV with little change in the beam current or divergence. This is
usually adequate to determine the instrument passband. Below 30 eV, and where
possible in other instances, the instrument response is completely character-
ized at a series of individual energies. The total response is then obtained
from the archived data.

B. Angular Divergence

The average angular divergence and uniformity at the beam is obtained
from the two independent RPAs which are at different distances from the ion
source. The aperture of both units is aligned with the axis of the drift
tube. Figure 8 shows typical values of the measured average divergence over
the range of energies of interest. The average divergence value holds rela-
tively constant from 50 eV to 5 eV. Below that, the beam expands due to the
weak focusing effects of the electrostatic mirrors, the increasing importance
to the transverse velocity component, and the generally increased effect of
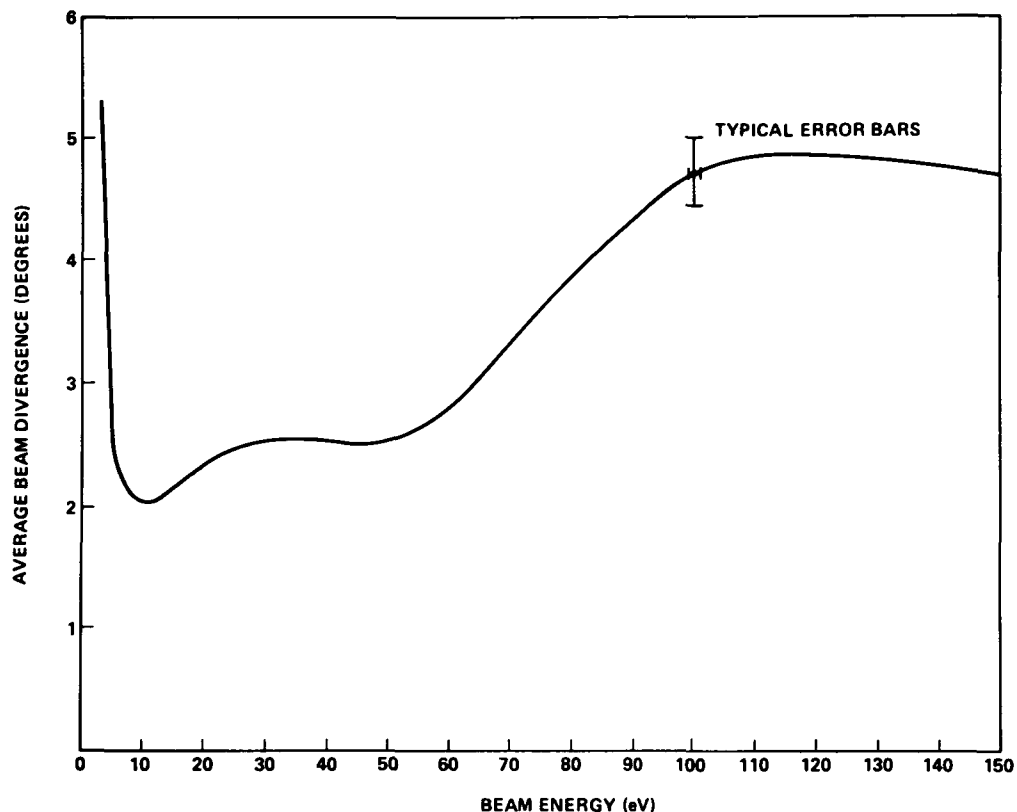charge images and fringing fields.

13

Figure 8. Average beam divergence vs. beam energy.

C. Beam Uniformity

The beam delivered to the test instrument when adjusted to minimum divergence is relatively constant, ~10%, over a 10-cm-diameter circle when the beam energy is greater than 5 eV. Below this energy, the spread increases to about 5 deg at 1.5 eV. After the system is at operating temperature, the stability without feedback is about 5% drift in beam current per 30 min. This can be reduced almost arbitrarily with active feedback; however, the usual procedure is to simply monitor the actual value for later calibration.

D. Beam Purity

In order to function at these low energies, no mass resolution is used in the generation system. Some control is possible by adjusting the ionizer bias to optimize the desired reaction cross section. Instead, the actual beam is analyzed as it is delivered to the instrument. Figure 9 shows a typical beam spectrogram using N_2 as the working gas. The largest impurity, ~3%, is at a Q/M of 14, and is essentially fixed by the relative ionization cross sections. The other impurities are basically set by background impurities in the chamber and gas sources.
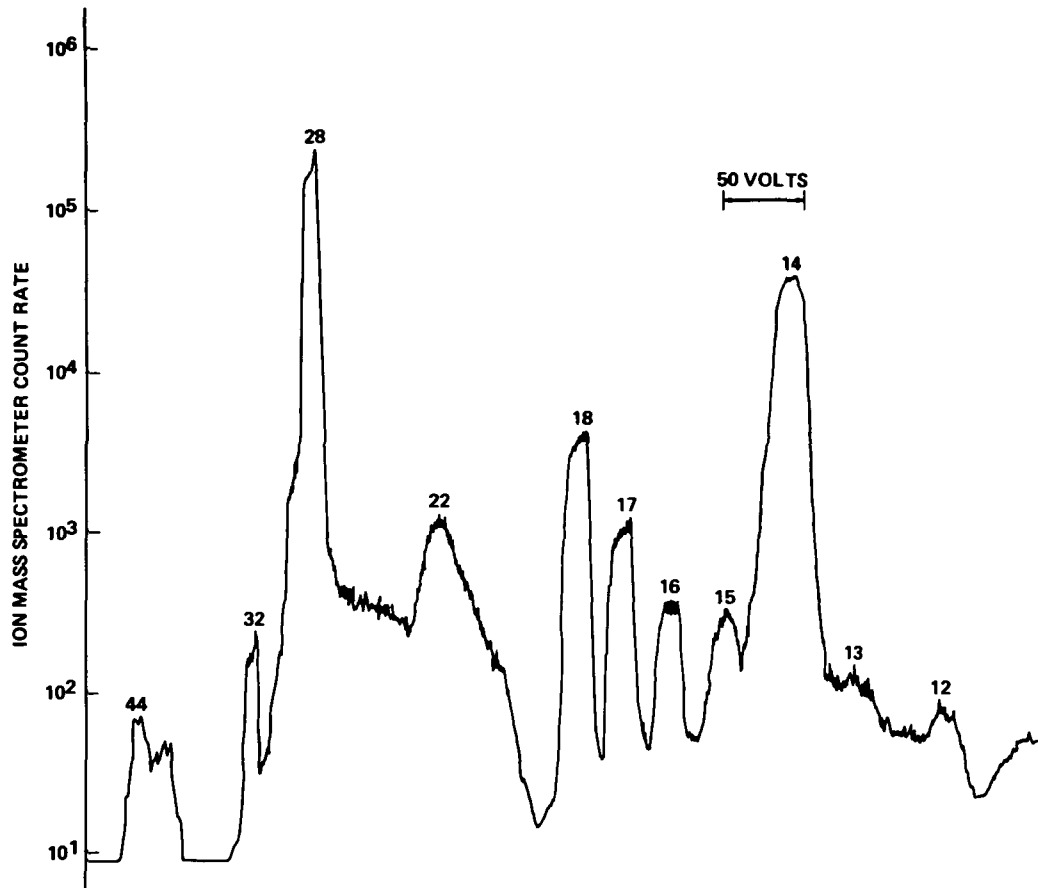
14

Figure 9. Typical ion mass spectrogram of ion source output
using N_2 working gas.

IV. CALIBRATION PROCEDURE

The instrument or component being processed is mounted on the tilt/ translation table approximately 44 cm below the drift tube aperture. The position of the instrument is adjusted so that the tilt and rotation axis are both in the plane of the instrument aperture. While the exact procedure is somewhat dependent on the type of instrument under test, the typical procedure is as follows: The energy and beam current desired are chosen. The computer then consults an interpolated lookup table with preset limits on the allowable variation of each of the parameters to be set. The computer then makes optimizing adjustments until stability at the new parameters is achieved. Operator intervention allows these tables to be overridden for special cases. The time required for this is usually less than 30 min, and depends principally on how large an excursion is made from the last value. Next the instrument is stepped through a preset number of angular steps, with the beam being characterized before, during, and after each set of data. The instrument is then rotated, and the process repeated.

In principle, and to a large extent in practice, a full instrument scan can be obtained with only operator monitoring. Full automation requires the prior coordination of the source and instrument data streams. This is gen-

15

erally performed by means of a standard RS-232 interface between the ground support for the instrument and the LEIF computer. At each calibration point, the data appropriate to the instrument are output as a data file which is archived with a simultaneous parameter file from the chamber, such as beam current, energy spread, and instrument orientation. Alternatively, hard copy of the beam parameters is available for more traditional procedures. An array of uncommitted analog and digital inputs and outputs is available for special purposes, or for use when dedicated ground support equipment is not justified. The microcomputer, utilizing a 68,000 CPU, possess sufficient speed to support both the chamber and instrument operation in most cases.

REFERENCES

1. Biddle, A. P., Moore, T. E., and Chappell, C. R.: Evidence for Ion Heat Flux in the Light Ion Polar Wind. J. Geophys. Res., Vol. 90, 1985, pp. 8552-8558.

2. Gallagher, D. L., Menietti, J. D., Burch, J. L., Persoon, A. M., Waite, J. H., Jr., and Chappell, C. R.: Evidence of High Densities in the Polar Cap During the Recovery Phase. In press, J. Geophys. Res., 1985.

3. Nagai, T., Waite, J. H., Jr., Green, J. L., Chappell, C. R., Olsen, R. C., and Comfort, R. H.: First Measurements of Supersonic Polar Wind in the Polar Magnetosphere. Geophys. Res. Lett., Vol. 11, 1984, pp. 669-672.

4. Chappell, C. R., Fields, S. A., Baugher, C. R., Hoffman, J. H., Hanson, W. B., Wright, W. W., Hammack, H. D., Carignan, G. R., and Nagy, A. F.: The Retarding Ion Mass Spectrometer on Dynamics Explorer-A. Space Sci. Instrum., Vol. 5, 1981, pp. 477-491.

5. Olsen, R. C.: Modification of Spacecraft Potentials by Plasma Emission. J. Spacecraft & Rockets, Vol. 18, 1981, p. 462.

6. Singh, N. and Baugher, C. R.: Sheath Effects on Current Collection by Particle Detectors with Narrow Acceptance Angles. Space Sci. Instrum., Vol. 5, 1981, p. 295.

7. Comfort, R. H., Baugher, C. R., and Chappell, C. R.: Use of the Thin Sheath Approximation for Obtaining Ion Temperatures from the ISEE 1 Limited Aperture RPA. J. Geophys. Res., Vol. 87, 1982, pp. 5109-5123.

8. Gewartowski, J. W. and Watson, H. A.: Principles of Electron Tubes. D. Van Nostrand Company, Inc., 1985.

9. Goldan, P. D., Yadlowsky, E. J., and Whipple, E. C., Jr.: Errors in Ion and Electron Temperature Measurements due to Grid Plane Potential Non-uniformities in Retarding Potential Analyzers. J. Geophys. Res., Vol. 78, 1973, p. 2907.

10. Reasoner, D. L., Chappell, C. R., Fields, S. A., and Lewter, W. J.: Light Ion Mass Spectrometer for Space Plasma Investigations. Rev. Sci. Instrum., Vol. 53, 1982, p. 441.

11. Kaufman, H. R. and Reader, P. D.: In Electrostatic Propulsion. Edited by D. B. Langmuir, E. Stuhlinger, and J. M. Selle, Academic Press, New York, 1961, pp. 3-20.

12. Banks, P. M. and Kockarts, G.: Aeronomy, Part A. Academic Press, New York, 1973.

13. D'Angelo, N. and Alport, M. J. Alport: On "Anomalously" High Ion Temperatures in Plasma Discharges. Plasma Physics, Vol. 24, 1982, p. 1291.

14. Troy, B. E., Jr. and Maier, E. J.: Effect of Grid Transparency and Finite Collector Size on Determining Ion Temperature and Density on the Retarding Potential Analyzer. J. Geophys. Res., Vol. 80, 1975, p. 2236.

15. Hanson, W. B., Frame, D. R., and Midgley, J. E.: Errors in Retarding Potential Analyzers Caused by Non-Uniformity of the Grid Plane Potential. J. Geophys. Res., Vol. 77, 1972, p. 1914.

16. Biddle, A. P., Reynolds, J. M., Chisholm, W. L., Jr., and Hunt, R. D.: The Marshall Space Flight Center Low-Energy Ion Facility - A Preliminary Report. NASA TM-82559, October 1983.

17. Aston, G. and Kaufman, H. R.: Ion Beam Divergence Characteristics of Three-Grid Accelerator Systems. AIAA Journal, Vol. 17, 1979, p. 64.

18. Newrock, R. S.: An IEEE-488 Bus Tutorial. Microsystems, April 1983, p. 60.

19. Green, J. L. and Peters, D. J. Peters (editors): Introduction to the Space Physics Analysis Network (SPAN) - First Edition. NASA TM-86499, April 1985.

APPROVAL

AN INTEGRATED DEVELOPMENT FACILITY FOR THE CALIBRATION
OF LOW-ENERGY CHARGED PARTICLE FLIGHT INSTRUMENTATION -
CENTER DIRECTOR'S DISCRETIONARY FUND FINAL REPORT

By Alan P. Biddle and John M. Reynolds

The information in this report has been reviewed for technical content. Review of any information concerning Department of Defense or nuclear energy activities or programs has been made by the MSFC Security Classification Officer. This report, in its entirety, has been determined to be unclassified.

A. J. DESSLER
Director, Space Science Laboratory